

Fabricating centimeter-scale high quality factor two-dimensional periodic photonic crystal slabs

Jeongwon Lee,^{1,*} Bo Zhen,¹ Song-Liang Chua,¹ Ofer Shapira,¹ and Marin Soljačić¹

¹Research Laboratory of Electronics, Massachusetts Institute of Technology,
77 Massachusetts Avenue, Cambridge, Massachusetts 02139, USA

[*jeongwon@mit.edu](mailto:jeongwon@mit.edu)

Abstract: We present a fabrication route for centimeter-scale two-dimensional defect-free photonic crystal slabs with quality factors bigger than 10,000 in the visible, together with a unique way to quantify their quality factors. We fabricate Si₃N₄ photonic crystal slabs, and perform an angle-resolved reflection measurement. This measurement data is used to retrieve the quality factors of the slabs by fitting it to a model based on temporal coupled-mode theory. The macroscopic nature of the structure and the high quality factors of their resonances could open up new opportunities for realizing efficient macroscale optoelectronic devices such as sensors, lasers, and energy harvesting systems.

© 2014 Optical Society of America

OCIS codes: (220.0220) Optical design and fabrication; (220.4241) Nanostructure fabrication.

References and links

1. K. J. Vahala, "Optical microcavities" *Nature* **424**, 839–846 (2003).
2. T. Benson, S. Boriskina, P. Sewell, A. Vukovic, S. Greedy, and A. Nosich, "Micro-optical resonators for micro-lasers and integrated optoelectronics" (Springer Netherlands, 2006), vol. 216 of *Frontiers in Planar Lightwave Circuit Technology*, pp. 39–70.
3. D. K. Armani, T. J. Kippenberg, S. M. Spillane, and K. J. Vahala, "Ultra-high-q toroid microcavity on a chip" *Nature* **421**, 925–928 (2003).
4. J. Zhu, S. K. Ozdemir, Y.-F. Xiao, L. Li, L. He, D.-R. Chen, and L. Yang, "On-chip single nanoparticle detection and sizing by mode splitting in an ultrahigh-q microresonator" *Nat. Photon.* **4**, 46–49 (2010).
5. O. Painter, R. K. Lee, A. Scherer, A. Yariv, J. D. O'Brien, P. D. Dapkus, and I. Kim, "Two-dimensional photonic band-gap defect mode laser" *Science* **284**, 1819–1821 (1999).
6. M. Nomura, S. Iwamoto, K. Watanabe, N. Kumagai, Y. Nakata, S. Ishida, and Y. Arakawa, "Room temperature continuous-wave lasing in photonic crystal nanocavity" *Opt. Express* **14**, 6308–6315 (2006).
7. C. Monat, C. Seassal, X. Letartre, P. Regreny, P. Rojo-Romeo, P. Viktorovitch, M. L. V. d'Yerville, D. Cassagne, J. P. Albert, E. Jalaguier, S. Pocas, and B. Aspar, "InP-based two-dimensional photonic crystal on silicon: In-plane bloch mode laser" *Appl. Phys. Lett.* **81**, 5102–5104 (2002).
8. H.-Y. Ryu, S.-H. Kwon, Y.-J. Lee, Y.-H. Lee, and J.-S. Kim, "Very-low-threshold photonic band-edge lasers from free-standing triangular photonic crystal slabs" *Appl. Phys. Lett.* **80**, 3476–3478 (2002).
9. S. Kim, S. Ahn, J. Lee, H. Jeon, P. Regreny, C. Seassal, E. Augendre, and L. D. Cioccio, "Milliwatt-level fiber-coupled laser power from photonic crystal band-edge laser" *Opt. Express* **19**, 2105–2110 (2011).
10. B.-S. Song, S. Noda, T. Asano, and Y. Akahane, "Ultra-high-q photonic double-heterostructure nanocavity" *Nat. Mater.* **4**, 207–210 (2005).
11. Y. Takahashi, Y. Tanaka, H. Hagino, T. Sugiya, Y. Sato, T. Asano, and S. Noda, "Design and demonstration of high-q photonic heterostructure nanocavities suitable for integration" *Opt. Express* **17**, 18093–18102 (2009).
12. A. M. Armani, R. P. Kulkarni, S. E. Fraser, R. C. Flagan, and K. J. Vahala, "Label-free, single-molecule detection with optical microcavities" *Science* **317**, 783–787 (2007).

13. T. Barwicz, M. Popović, P. Rakich, M. Watts, H. Haus, E. Ippen, and H. Smith, "Microring-resonator-based add-drop filters in silicon: fabrication and analysis" *Opt. Express* **12**, 1437–1442 (2004).
14. T. Barwicz, M. Popović, M. R. Watts, P. T. Rakich, E. P. Ippen, and H. I. Smith, "Fabrication of add-drop filters based on frequency-matched microring resonators" *J. Lightwave Technol.* **24**, 2207–2218 (2006).
15. J. Lee, B. Zhen, S. L. Chua, W. Qiu, J. D. Joannopoulos, M. Soljačić, and O. Shapira, "Observation and differentiation of unique high- q optical resonances near zero wave vector in macroscopic photonic crystal slabs" *Phys. Rev. Lett.* **109**, 067401 (2012).
16. C. P. Fucetola, H. Korre, and K. K. Berggren, "Low-cost interference lithography" *J. Vac. Sci. Technol.*, **B 27**, 2958–2961 (2009).
17. Q. Xie, M. H. Hong, H. L. Tan, G. X. Chen, L. P. Shi, and T. C. Chong, "Fabrication of nanostructures with laser interference lithography" *J. Alloys Compd.* **449**, 261–264 (2008).
18. H. I. Smith, "Low cost nanolithography with nanoaccuracy" *Physica E* **11**, 104–109 (2001).
19. J. Hu, N.-N. Feng, N. Carlie, L. Petit, A. Agarwal, K. Richardson, and L. Kimerling, "Optical loss reduction in high-index-contrast chalcogenide glass waveguides via thermal reflow" *Opt. Express* **18**, 1469–1478 (2010).
20. A. F. Oskooi, D. Roundy, M. Ibanescu, P. Bermel, J. D. Joannopoulos, and S. G. Johnson, "Meep: A flexible free-software package for electromagnetic simulations by the fdtd method" *Comput. Phys. Commun.* **181**, 687–702 (2010).
21. A. Buxbaum and M. W. Montgomery, U.S. Patent No. 6,582,861 B2 (24 Jun. 2003).
22. S.-L. Chua, Y. Chong, A. D. Stone, M. Soljacic, and J. Bravo-Abad, "Low-threshold lasing action in photonic crystal slabs enabled by fano resonances" *Opt. Express* **19**, 1539–1562 (2011).
23. L. Ferrier, P. Rojo-Romeo, E. Drouard, X. Letatre, and P. Viktorovitch, "Slow bloch mode confinement in 2d photonic crystals for surface operating devices" *Opt. Express* **16**, 3136–3145 (2008).
24. M. Galli, M. Agio, L. C. Andreani, M. Belotti, G. Guizzetti, F. Marabelli, M. Patrini, P. Bettotti, L. D. Negro, Z. Gaburro, L. Pavesi, A. Lui, and P. Bellutti, "Spectroscopy of photonic bands in macroporous silicon photonic crystals" *Phys. Rev. B* **65**, 113111 (2002).
25. A. R. Alija, L. J. Martínez, P. A. Postigo, J. Sánchez-Dehesa, M. Galli, A. Politi, M. Patrini, L. C. Andreani, C. Seassal, and P. Viktorovitch, "Theoretical and experimental study of the suzuki-phase photonic crystal lattice by angle-resolved photoluminescence spectroscopy" *Opt. Express* **15**, 704–713 (2007).
26. M. Gehl, R. Gibson, J. Hendrickson, A. Homyk, A. Säynätjoki, T. Alasaarela, L. Karvonen, A. Tervonen, S. Honkanen, S. Zandbergen, B. C. Richards, J. D. Olitzky, A. Scherer, G. Khitrova, H. M. Gibbs, J.-Y. Kim, and Y.-H. Lee, "Effect of atomic layer deposition on the quality factor of silicon nanobeam cavities" *J. Opt. Soc. Am. B* **29**, A55–A59 (2012).
27. E. Jaquay, L. J. Martínez, C. A. Mejia, and M. L. Povinelli, "Light-assisted, templated self-assembly using a photonic-crystal slab" *Nano Letters* **13**, 2290–2294 (2013).

1. Introduction

High quality factor (Q) micro-resonators [1, 2], characterized by narrow resonance line widths and long photon storage time, are excellent candidates for sensors with enhanced detection sensitivity [3, 4] and efficient laser cavities using defect modes [5, 6] or extended modes [7–9]. In such practical device applications, it is desirable to realize high Q resonators with simultaneously large areas and wide free spectral ranges (FSRs). Cavities with large areas are desirable to trap sufficient energy for realizing sensing and energy harvesting. In addition, a wide FSR ensures that adjacent discrete cavity modes are well separated in order to promote single-mode operation. Several very high Q micro-resonators such as defects in photonic crystals (PhCs) [5, 6, 10, 11], micro-toroids [3, 4, 12], and micro-ring resonators [13, 14] have been extensively studied over the past few decades. However, defect PhC devices have very small sizes, and while micro-toroids and rings are typically larger, their FSRs are fairly narrow. In this paper, as an extension of our previous study [15], we demonstrate optimized fabrication of a centimeter scale 2D defect-free PhC through which we obtained increased Q by a factor of three. Thus, the final samples possess high Q , large area, and wide FSR. By analyzing the resonances of our structure through reflectivity measurement over a broad frequency range, the pattern quality was quantified in terms of Q . This Q reflects not only the surface roughness and pattern shape, but also the sidewall roughness and the nanometer scale variation of the pattern properties over the whole structure, such as periodicity and hole sizes. Therefore, Q can systematically quantify the average quality of millions of periodic patterns over a centimeter scale,

which is not feasible to do by characterizing a localized nanometer scale area with atomic force microscopy (AFM) or scanning electron microscope (SEM).

2. Fabrication process

To achieve high Q resonances in the visible wavelength range, both the bulk material properties and the nanoscale geometry have to be considered. Experimentally attainable Q is bounded by bulk material absorption. A LPCVD-deposited Si_3N_4 layer on top of a 6 μm thick SiO_2 layer on Si substrate is used in this study. Through an absorption test enabled by a prism coupler, Q limited by bulk materials absorption is found to be 5×10^5 at $\lambda = 633 \text{ nm}$. The same test was used to measure its refractive index. With a refractive index of 2.02, Si_3N_4 forms sufficient index contrast with SiO_2 (index of 1.45) below and air or fluids on top, so more than 80% of the mode energy is confined within this Si_3N_4 layer with thickness of less than 200nm. The fabrication process consists of deposition of a quadlayer resist stack, pattern definition by interference lithography (IL) [16], pattern transfer by reactive ion etching (RIE), and removal of the remaining resist. Fig. 1 shows the schematic outline of the fabrication process. The quadlayer is comprised of a layer of antireflection coating (ARC, XHRiC-16), a thin layer of SiO_2 deposited by electron beam evaporation, a negative photoresist (PR, THMR-iN PS-4), and another thin layer of ARC (ARC', XHRiC-16). XHRiC-16 is an ARC material specifically designed for dry etching processes, which makes metal hard masks unnecessary. Metal hard masks are robust, but even a very small amount of metal residue substantially increases light absorption and therefore limits the highest achievable Q 's. XHRiC-16 is robust enough to etch several hundred nanometers of Si_3N_4 and eliminates any potential metal contamination. ARC is introduced to limit the amount of light reflected back into the PR layer. Otherwise, this reflected light will form a vertical standing wave with the incident light, which causes poor sidewall profiles in the PR layer. The thickness of the ARC layer is optimized to minimize the reflection at the bottom of the PR layer. Together with another thin layer of ARC (ARC') on top of the PR layer, the reflection can be further reduced, as shown in Fig. 1(e). It reduces the overall reflection by roughly a factor of two and the minimum reflection by a factor of one hundred, which provides tolerance to an increase in reflectivity from a small deviation in the thickness of each layer of the resist stack. The SiO_2 layer is used as a hard mask while the ARC layer is etched.

After the deposition of the resist stack, IL uses a 325 nm He/Cd laser to define the 2D periodic pattern on the PR layer. The laser beam is split into two mutually coherent beams, and the angle between the two beams determines the periodicity of the pattern. A single exposure defines a 1D grating pattern, and a following perpendicular exposure defines the 2D square array pattern [17]. The shape and the size of the holes after development are determined by the exposure time. Short exposure results in large diamond shape holes, and long exposure results in small circular shape holes. Optimal exposure typically produces round holes with a diameter to periodicity ratio (d/a) of 0.3-0.5. The ratio, d/a , is 0.5 in this study. Two types of IL systems are explored in this paper: Lloyds mirror (LM) and Mach-Zehnder (MZ) [18]. Higher Q 's were observed from the samples exposed using MZ. The comparison between the two IL systems will be further discussed in a later section.

The exposed PR is hard baked (110 $^\circ\text{C}$, 90 sec) and developed in a commercial developer CD-26 (20 $^\circ\text{C}$, 60 sec). The image of a 4-inch wafer after development is shown in Fig. 2(b). The 2D periodic pattern on the PR layer produced a diffraction pattern when two external fiber light beams illuminating it. Then, the PR pattern is transferred to the Si_3N_4 layer using RIE (Plasmatherm 790). The two ARC layers are etched with $\text{He}:\text{O}_2 = 16:8 \text{ sccm}$ (10 mTorr, 200 V), and SiO_2 and Si_3N_4 are etched with $\text{CHF}_3:\text{O}_2 = 16:3 \text{ sccm}$ (10 mTorr, 400 V). After the RIE steps, the remaining ARC layer is removed completely by immersion into a commercial

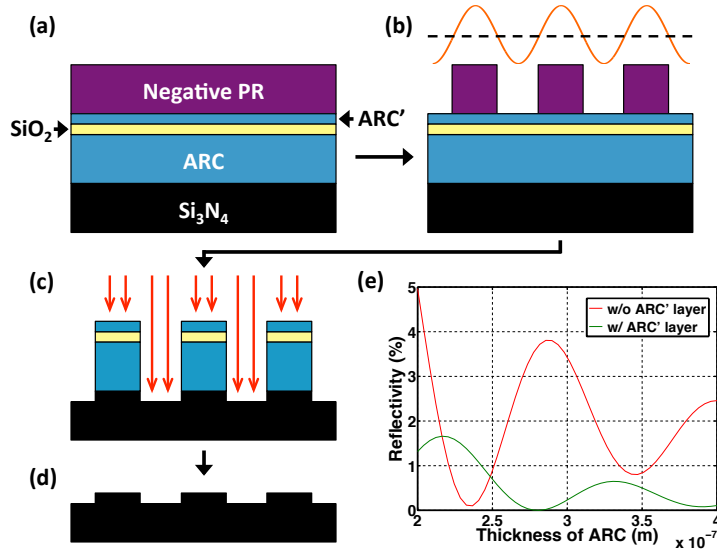


Fig. 1. (a)-(d) Schematic outline of the process flow: (a) Deposition of the resist layers, where ARC' stands for a thin ARC layer, (b) pattern definition by interference lithography followed by development, (c) pattern transfer to the Si_3N_4 layer by RIE, (d) removal of remaining resist stack. (e) Reflectivity at the bottom of the PR layer as a function of the thickness of the ARC layer. It is important to minimize the amount of light reflected back into the PR layer because it forms a vertical standing wave with the incident light. This produces poor sidewall profiles after development, and hence low Q 's of resonances. The green and red curves represent the reflectivity with and without 45 nm of ARC' layer, respectively. The existence of the ARC' layer reduced overall reflectivity by roughly half and so did the minimum reflectivity by a factor of one hundred.

post-etch residue remover EKC-265. A top-view SEM image of the final PhC structure is shown in Fig. 2(c). Higher Q 's were observed when the PR after development is descummed using O_2 RIE. This descumming step smoothens the wavy sidewalls of the PR pattern, allowing more anisotropic pattern transfer afterwards. This step will be further discussed in a later section.

3. Sample characterization

The characterization of the PhC slab is performed when the light from a supercontinuum laser source (SuperK Compact, NKT Photonics) is reflected from the sample, and this light is recorded with a high resolution (up to 0.06\AA) scanning monochromator (1250M, HORIBA) at small incident angles ($0-0.5^\circ$). The measurement setup is illustrated in Fig. 2(a). The sample was placed in a precision demountable liquid cell containing methanol, and the whole cell was mounted on a motorized rotational stage (ESP300, Newport). The methanol intermediate layer (index of 1.33) was used to lower index contrast between Si_3N_4 PhC slab and its environment, thus associated scattering loss [19]. To corroborate experimental results, finite difference time domain simulation, MEEP [20], was performed to calculate the modes of the PhC. Figs. 3(a) and 3(b) show the simulation and the experimental results, respectively.

Fig. 3(a) is the band diagram of the PhC. Wave vector k is converted to angles on the y-axis while the frequency is represented by the x-axis. Calculated Q_{rad} of each mode is also shown in the plot. The singly degenerate mode has infinite Q_{rad} at Γ , while the doubly degenerate mode has finite Q_{rad} at Γ and split into two modes as k -point moves away from Γ towards X [15]. Fig.

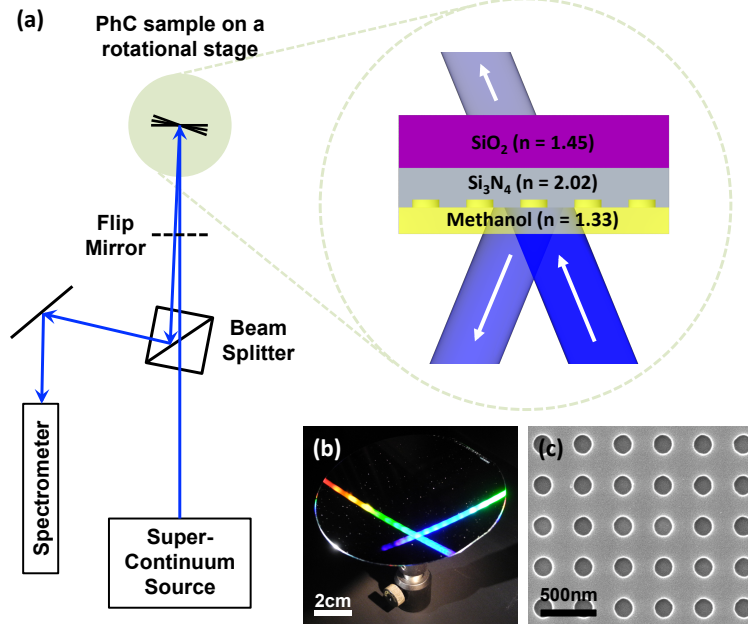


Fig. 2. (a) Schematic drawing of the reflectivity measurement setup. Enlarged view of reflection path of light from the PhC sample is also represented on the right. (b) Image of an exposed 4-inch wafer after development. The two diffraction beams were produced by two fiber light beams. This shows the 2D periodic pattern was defined over the entire area of the wafer. (c) Top-view scanning electron micrograph of the final sample with periodicity of 375 nm.

3(b) is the reflectivity measurement result at $\theta = 0.2^\circ$. In Fig. 3(a), the doubly degenerate mode starts to split at $\theta = 0.2^\circ$, and this was experimentally observed, as shown in Fig. 3(b). Also, the spacing between the doubly degenerate (or low Q) mode and the singly degenerate (or high Q) Fano resonant mode in Fig. 3(a) and the one in Fig. 3(b) agree well with each other.

As the reflectivity measurement approaches $\theta = 0^\circ$, the observed Q^{total} (where $1/Q^{\text{total}} = 1/Q_{\text{rad}} + 1/Q_{\text{loss}}$) of a high Q Fano resonant mode can be approximated to be the same as Q_{loss} . In this way, the degree of fabrication imperfections was quantified in terms of Q^{total} . This is a valid approximation because Q_{rad} of the high Q mode diverges as k -point moves toward Γ , while Q_{loss} was found to be almost constant [15]. The sidewall roughness and variations in periodicity and size of holes are taken into account in the Q^{total} , as well as the surface roughness and pattern shape. Therefore, this approach enables measurement of the average quality of overall PhC structure, while the common visual analysis tools such as AFM or SEM provide quantitative descriptions of microstructure details. Note that, however, the exact origin of Q_{loss} is hard to trace using this approach. Q limited by the divergence angle of the incident beam is in the order of 10^6 , which is also much higher than Q_{loss} .

Q^{total} of the sample is retrieved by fitting Eq. (1) to the reflectivity measurement data. This formula has previously been derived from temporal coupled mode theory [15].

$$|r_{\text{PhC}}|^2 = \left| r_d - \frac{\gamma_t \cdot (\gamma_t r_d + \gamma_b t_d)}{i(\omega - \omega_0) + \gamma_t^2/2 + \gamma_b^2/2 + 1/\tau_{\text{loss}}} \right|^2 \quad (1)$$

r_d and t_d are the complex reflection and transmission coefficients of the sample without the 2D pattern, which can be obtained by fitting the background data (Blue line). γ_t and γ_b are the

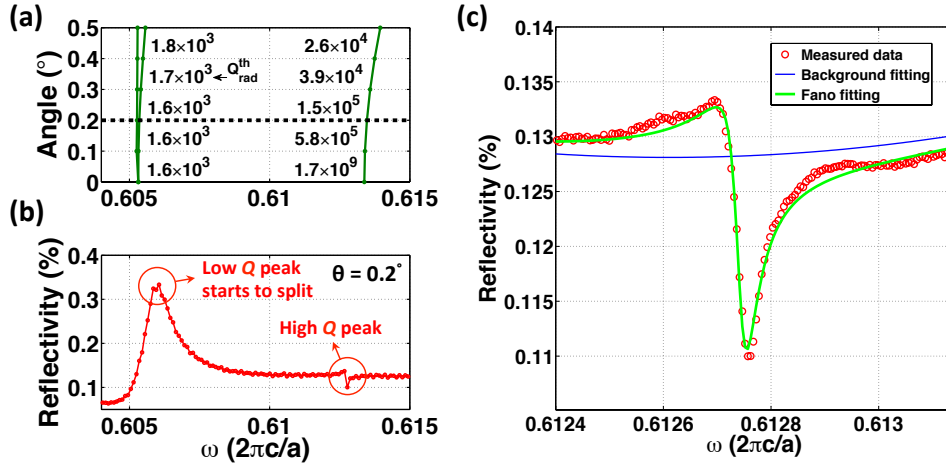


Fig. 3. (a) The band diagram calculated with MEEP. The frequency is plotted along the x-axis, and the wave vector is converted to the angle and plotted along the y-axis. The numbers inside the graph ($Q_{\text{rad}}^{\text{th}}$) represent the theoretical radiative quality factors of each mode calculated with MEEP. The two lines on the left are low Q modes degenerated at the Γ point, and the line on the right is a high Q mode whose radiative Q diverges at the Γ point. (b) Experimental reflectivity data measured at 0.2° . The frequencies of the peaks agree well with the calculation result. (c) The high Q peak in (b) was measured again with a higher resolution, and the data was fitted to the reflectivity formula derived from coupled mode theory. The red dots are the measured data, the blue curve is the fitted background, and the green curve is the final fitting result.

coupling strengths of the resonant mode to the top (Methanol) and the bottom (SiO_2) layers, respectively. ω_0 and $1/\tau_{\text{loss}}$ are center frequency of the resonance and resonant energy decay rate due to fabrication imperfections. These four parameters are fitted using a non-linear least squares method (Green line) and used to compute Q^{total} . The fitting process is shown Fig. 3(c). Table 1 shows Q^{total} obtained from PhC slabs fabricated with various methods and hole depth. The standard error of fitted Q^{total} is 2%. The thickness of Si_3N_4 layer was 180 nm, and the holes were etched to the depth of 60, 120, and 180 nm. The accuracy of hole depth is approximately ± 5 nm. In general, deeper hole depths resulted in lower Q because of longer RIE step.

Table 1. Fitted Q^{total} of various PhC samples.

Q^{total}	Hole Depth		
	60nm	120nm	180nm
Lloyd's Mirror	10K	$O(10^3)$	$O(10^2)$
Mach-Zehnder	16K	14K	9K
Optimized Mach-Zehnder	32K	19K	17K
E-beam	10K	7K	6K

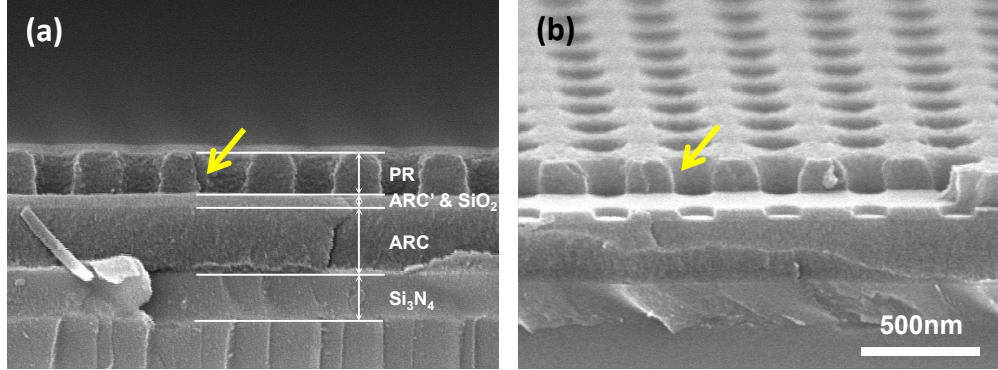


Fig. 4. (a) After development, sidewall profiles were wavy and slanted. (b) After O_2 RIE process, sidewall profiles became more vertical and straight.

4. Discussion

IL is a fast, inexpensive, and maskless lithography method; therefore, it is an optimal choice to fabricate large area periodic patterns. We studied two IL systems: LM and MZ [18]. Both systems share the same principle: formation of a standing wave with two mutually coherent laser beams. The MZ setup has a piezo sensor which recognizes and minimizes even very small vibrations. MZ can also expose larger size substrates. As shown in Fig. 2(b), the entire 4-inch wafer can be exposed with a single exposure. Therefore, it provides a high throughput as well as ease of quality control. Since all samples produced from the same exposure have the same degree of exposure quality, we were able to determine whether Q measured from the PhC is attributed to the exposure or other factors. In contrast, in the LM setup, each piece has to be exposed one by one, resulting in varying degree of exposure quality. In table 1, PhCs fabricated from LM showed Q of 10K [15], but the ones from MZ (other conditions were not changed) showed Q of 16K.

As shown in Fig. 4(a), PR sidewalls were wavy and not perfectly vertical after development. Common positive PRs that do not cross-link may be heated up to their softening point and reflowed. However, because most negative PRs (including THMR-iN PS-4) cross-link, they cannot be smoothed out through a reflow process. Therefore, O_2 RIE was used to make the sidewalls of the PR layer more even and vertical, as shown in Fig. 4(b) [21]. This allows more anisotropic etching in the subsequent layers. Improvements in the Q 's were observed when this step was implemented. This O_2 RIE etches the ARC' layer at the same time. Different gas compositions for SiO_2 and Si_3N_4 RIE were also studied. We confirmed that the mixture of $CHF_3:O_2 = 16:3$ results in higher Q than CF_4 gas [13]. After all of these optimization steps, Q of 32K was measured.

Lastly, we fabricated PhC slabs using electron beam lithography (F-125, Elionix). The pattern area was $600 \times 600 \mu m^2$, which is sufficiently large that Q is not limited by its pattern size [22, 23]. From [23], we predicted Q_{rad} limited by lateral size is approximately 6×10^5 , which is much higher than the measured Q values. Exposure took around 6 hours, but their Q 's were not higher than the ones fabricated using IL. By optimizing exposure conditions, Q can be further improved, but the low throughput and limited pattern area prevents electron beam lithography from being considered as the optimal candidate for large area high Q PhC fabrication.

5. Conclusion

In conclusion, we reported a centimeter scale large-area high- Q defect-free 2D PhC fabrication process and a unique way to measure and comprehensively quantify the quality of 2D PhC slabs. Our reflectivity measurement is similar to previous studies [24, 25] in that relatively simple optical measurement was performed to investigate the photonic band structures of the fabricated PhC samples. However, it is unique in that we further used temporal coupled mode theory to fit the reflectivity measurement data to extract Q^{total} . The fabrication steps that we established here improved Q by a factor of three from our previous study [15]. We further confirmed that IL is a more suitable method to fabricate macroscopically large PhCs in terms of cost and time efficiency, compared to e-beam lithography. Since theoretical $Q_{\text{rad}}^{\text{total}}$ is unbounded, improving the fabrication process can further enhance attainable Q in the future. For example, by expanding the IL laser beams to a wider angle or by shaping the beam profile to a more uniform distribution, spatial power distribution will become uniform, and spatial variation of the pattern will be decreased. Post-process thin dielectric film coating using atomic layer deposition might also improve Q [26]. Furthermore, the fabrication and measurement schemes presented in this paper can be universally used for other materials, structures, or purposes such as a hard mask for III-V semiconductor materials. Along with the fact that the 2D pattern studied here supports large area resonances with strong confinement near its surface and theoretically ultra-high Q , together with ease of incorporating into a system, this work could be utilized to realize biomolecular sensors, organic light emitting devices, large area lasers, energy conversion systems, and light-assisted templated self-assembly [27].

Acknowledgments

B.Z., and M.S., as well as the fabrication part of the work were partially supported by S3TEC, an Energy Frontier Research Center funded by the U.S. DOE, Office of Science, and Office of Basic Energy Sciences, under Grant No. DE-SC0001299. B.Z. and M.S. were also partially supported by the U.S. Army Research Office through the Institute for Soldier Nanotechnologies under Contract No. W911NF-13-D-0001. S.L.C. and J.L. were also partially supported by the MRSEC Program of the NSF under Award No. DMR-0819762. PhCs were fabricated at the Nanostructures Laboratory (NSL) at MIT, and monochromator measurements were done at Physics Junior Lab at MIT. We thank Dr. Timothy Savas for proposing the quadlayer resist stack, Dr. Sean Robinson for providing the monochromator setup, and Adrian Y. X. Yeng and Chia Wei Hsu for fruitful discussions.